Int. J. Multiphase Flow, Vol. 7, pp. 129–149, 1981
Printed in Great Britain

0301-9322/81/020129-21$02.00/0
Pergamon/Elsevier

THE UPWARD FLOW OF AIR BETWEEN TWO WATERFALLS: AN UNUSUAL CHOKED FLOW PROBLEM

H. C. SIMPSON, D. H. ROONEY and M. MEGAHED
Department of Thermodynamics and Fluid Mechanics, University of Strathclyde, Glasgow, Scotland

(*Received* 11 *March* 1980; *in revised form* 17 *September* 1980)

Abstract—An experimental and theoretical investigation of the effect of air rising between two opposed waterfalls is presented. It is found experimentally that as the air flow is increased, the waterfalls are drawn more closely together until a critical air flow rate is reached at which the waterfalls collapse together. A theoretical analysis of this phenomenon is presented and the collapse condition is shown to be analogous to the choked flow of air through a nozzle the cross-sectional area of which is strongly pressure dependent. This dependency results in a very low effective "sonic" velocity and "choked" flow and the theoretical predictions are in reasonable agreement with the experiment results. The relevance of this work to the PWR refill problem is discussed.

1. INTRODUCTION

This paper is concerned with the upward flow of air between two waterfalls with attention being focussed on (i) predicting the air flow condition at which the two waterfalls just come together (ii) describing the waterfall trajectories. The problem is essentially one of choked flow and can be compared with the adiabatic flow of air through a nozzle with flexible walls, the shape of the nozzle being dictated by the air flow. As such it is a two phase flow problem of particular interest.

The study arose from observations made during experimental work, concerning safety aspects of pressurised water reactors, being carried out for the U.K. Nuclear Installations Inspectorate. The experiments related to the effectiveness with which the emergency core cooling system water penetrated to the lower plenum during the refill stage of a loss of coolant accident (Rooney *et al.* 1977) and involved air (or steam) rising up a simulated downcomer annulus test section against the falling water. Three different test sections were used to represent different simulations of a downcomer annulus, progressing from the simple developed rectangular flow section indicated in figure 1 (phase 1 tests) to a more realistically 1/10 scale model of a PWR cylindrical annulus. Interest here is centred on the phase 1 test section, which has a tangential side entry for the water, with air as the upflowing fluid to eliminate condensation effects.

During these tests, when the water was introduced through the side entries it flowed down through the test section in the form of twin waterfalls, as indicated in figure 1. It was found that, for any particular inlet water flowrate, varying the air flowrate altered the water trajectories and eventually produced a condition at which the waterfalls were pulled together, this being the prelude to liquid hold-up† by the air and consequent bypassing of the inlet water to an outlet pipe. This paper presents a theoretical analysis for the air rising between the opposing waterfalls and compares predictions with experimental results.

2. EXPERIMENTAL WORK

A line diagram of the general apparatus and instrumentation points is shown in figure 2. Referring to this, in conjunction with figure 1, air was passed into the lower plenum tank, up through the test section (made from transparent polycarbonate) and then through the outlet pipe. The depth (d) of the test section was 25.4 mm, the breadth (b) 690 mm and the outlet pipe

†Various other terms are commonly used to describe this condition, such as bypass, bridging, flooding or entrainment.

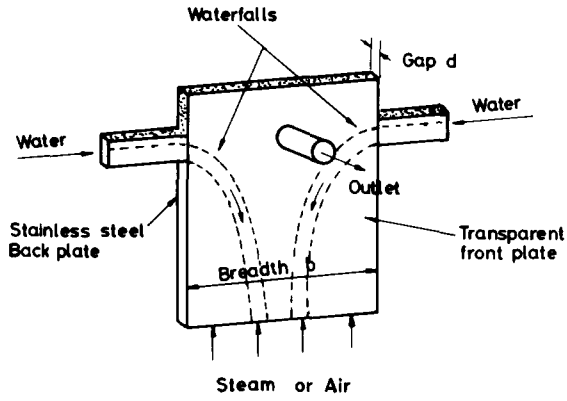

Figure 1. Test section for phase 1 tests—tangential entry.

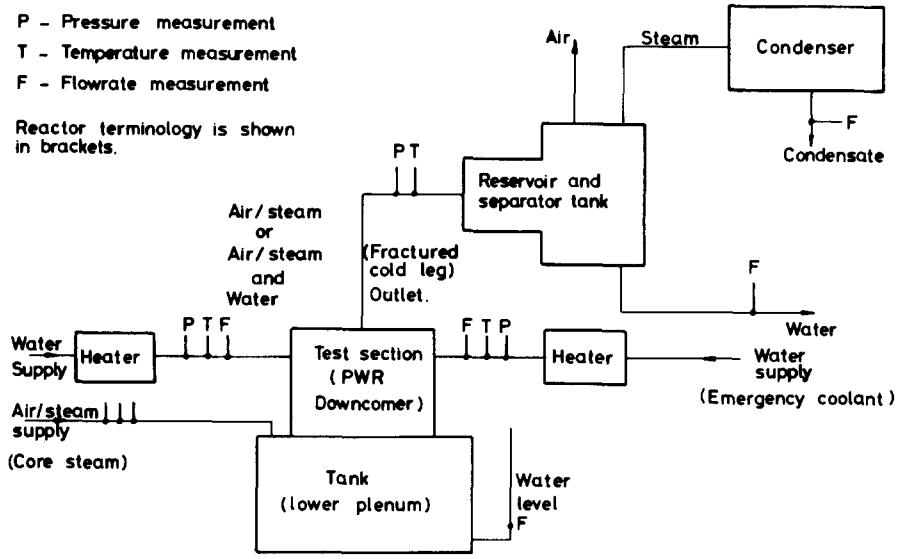

Figure 2. Line diagram of test rig showing instrumentation points.

diameter (d_0) 76 mm. A polycarbonate window was fitted to the lower tank so that flow behaviour could be observed there as well as in the test section.

The apparatus was used in an extensive experimental programme with steam–water and air–water interactions but only water-first tests with air are of relevance here. In a water-first test, a steady flow of water was introduced into the test section and then the air flow was increased in steps until water hold-up occurred, i.e. the water was bypassed from the inlets straight to the outlet without penetration to the lower plenum.

A series of such tests were carried out with the inlet water flow rate M_w varied in steps up to a maximum of 4.6 kg/s. Typical plots of the bypassed (or entrained) water flow rate M_{we} vs the upward air flow rate M_a are shown in figure 3. Four particular conditions which were encountered during any test are marked as positions *a*, *b*, *c* and *d* on figure 3, these being related to particular flow patterns within the test section. A more detailed representation of these flow patterns is given in figure 4 and can be described as follows. As the air rose between the two waterfalls, (a) the suction produced caused the two jets to come together (b) forming a barrier to the upward flow of air. It was then observed that the two waterfalls opened at the centre plane of the test section (see side views on figure 4) to form a passage for the upward rise of air moving against the downward film flow of water. A further increase in air flow caused the bridging of the two waterfalls to occur further up the test section

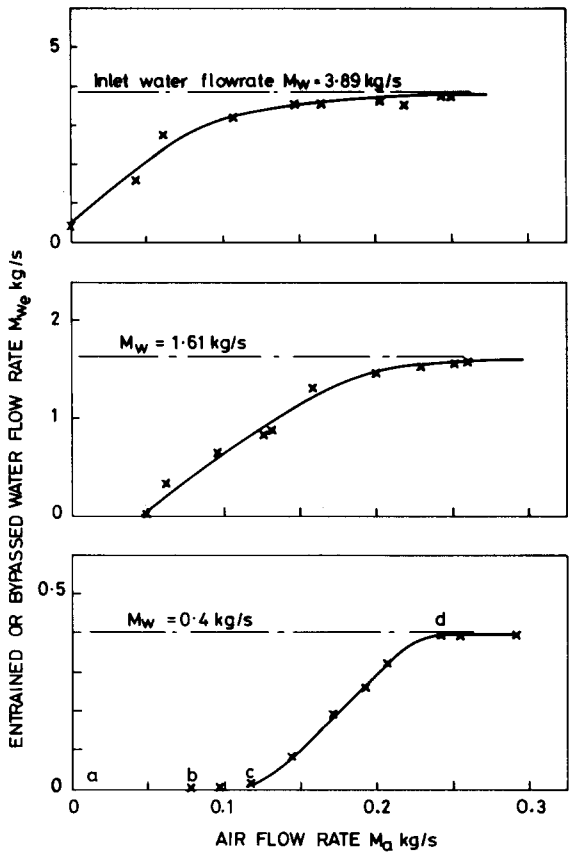

Figure 3. Typical bypass curves for air–water tests.

until ultimately the "bridge" reached the outlet hole (c) where water bypass started. A further increase in air flow increased the water entrainment or bypass effect until the waterfalls lost their identity and the air–water combination became a turbulent two-phase mixture in the test section (d) with none of the inlet water penetrating to the lower plenum. In this paper attention is centred on predicting condition (b) and on defining the waterfall trajectories.

Waterfall trajectories were measured using a cathetometer and telescope and typical results are shown in figure 5. The conditions under which the waterfalls were observed to come together at the bottom of the test section (i.e. condition b) are plotted in figure 6 in the form of air mass flow rate vs total water mass flow rate M_w. The curve is drawn as rising from the origin, although experimental data were not obtained at very low values of M_w; a theoretical justification for this is given later. Figure 6 does indicate a maximum value of M_a as M_w increases followed by a drop to zero as M_w is further increased. This final condition is due to the horizontal velocity component of the inlet water being sufficiently large as to cause the waterfalls to meet even with zero air flow.

3. THEORY

3.1 *The trajectories of the waterfall*

A simple theory for the trajectories of the waterfalls is presented here in which the drag of the water on the flat surfaces of the test section is neglected and the jet is assumed to be projected horizontally with a uniform initial velocity u_i and pressure p. Consider an element of the water jet of length ds and thickness k_w at point (x, z) and with velocity components u (in the x direction) and w (in the z direction) as shown in figure 7. Thus, if Δp is the pressure difference across the element ds, the equations of motion for the element of water of density ρ_w

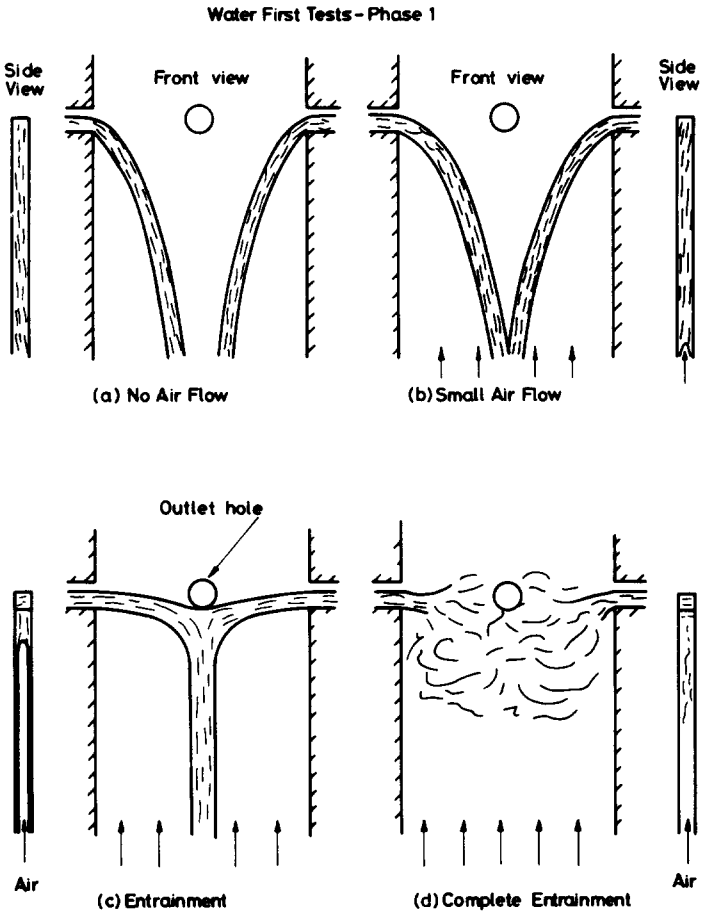

Figure 4. Air–water flow pattern representation.

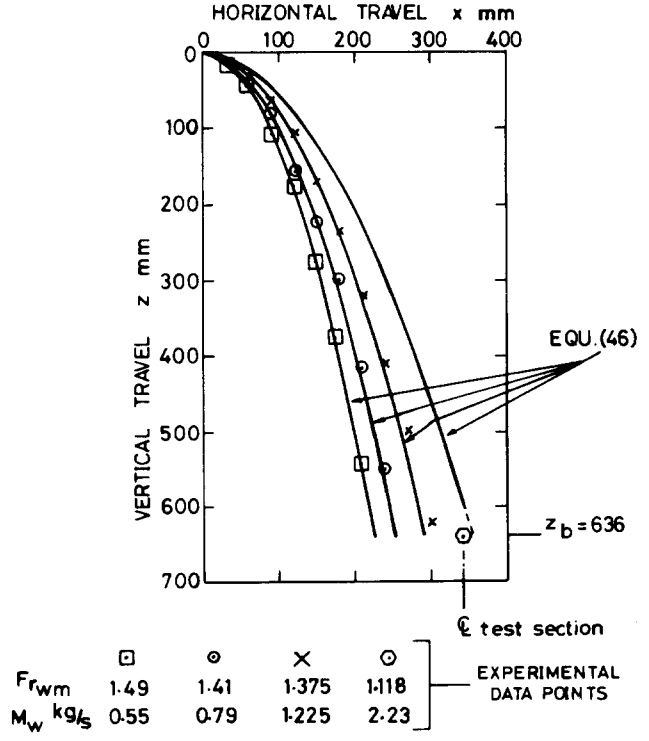

Figure 5. Typical waterfall trajectories—zero air flow.

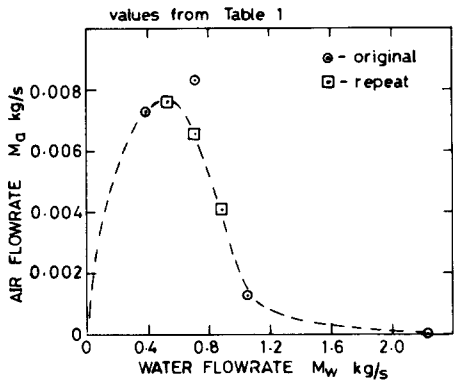

Figure 6. Experimental data for waterfall collapse.

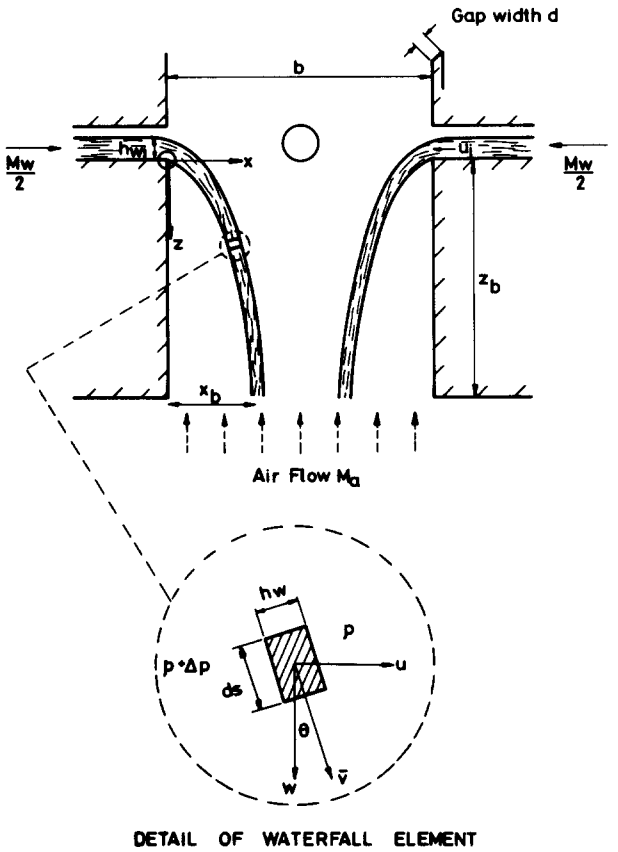

Figure 7. Co-ordinate system for waterfall analysis.

and local thickness h_w are,

$$\frac{du}{dt} = \left(\frac{\Delta p}{\rho_w h_w}\right) \frac{w}{(w^2+u^2)^{1/2}} \qquad [1]$$

$$\frac{dw}{dt} = g - \left(\frac{\Delta p}{\rho_w h_w}\right) \frac{u}{(w^2+u^2)^{1/2}}. \qquad [2]$$

Now from continuity

$$h_w \bar{v} = h_{wi} u_i \qquad [3]$$

where $\bar{v} = (u^2 + w^2)^{1/2}$ is the absolute velocity of the water element and h_{wi} and u_i are the thickness and velocity of the waterfall at the test section entry. It is then possible to solve [1]–[3] to give the velocities u, w and $\bar{v}$ by

$$\bar{v} = (2gz + u_i^2)^{1/2} \quad [4]$$

$$u = u_i + \frac{1}{\rho_w h_{wi} u_i} \int_0^z \Delta p \, dz \quad [5]$$

$$w = u_i \left[\left(1 + \frac{2g}{u_i^2} z\right) - \left(1 + \frac{1}{\rho_w h_{wi} u_i^2} \int_0^z \Delta p \, dz\right)^2 \right]^{1/2}. \quad [6]$$

Noting that the position (x, z) of the water element at any time t is given by the differential equation,

$$\frac{dx}{dz} = \frac{u}{w} \quad [7]$$

the equation of the water trajectory is obtained as,

$$x = \int_0^z \frac{dz}{\left[\dfrac{1 + (2g/u_i^2)z}{\left\{1 + \dfrac{1}{\rho_w h_{wi} u_i^2} \displaystyle\int_0^z \Delta p \, dz\right\}^2} - 1 \right]^{1/2}}. \quad [8]$$

This can be made dimensionless by defining the variables X and Z which are proportional to the reciprocal of Froude numbers and a dimensionless pressure difference ΔP as,

$$X = \frac{2g}{u_i^2} x; \quad Z = \frac{2g}{u_i^2} z; \quad \Delta P = \frac{\Delta p}{2g\rho_w h_{wi}} \quad [9]$$

giving,

$$X = \int_0^Z \frac{dZ}{\left[\dfrac{1 + Z}{\left\{1 + \displaystyle\int_0^z \Delta P \, dZ\right\}^2} - 1 \right]^{1/2}} \quad [10]$$

This is the general equation for the trajectory of each waterfall subjected to a gravitational force and a pressure difference which can vary from point to point along the trajectory. When $\Delta P = 0$, [10] reduces to the familiar parabolic form,

$$X = 2Z^{1/2}. \quad [11]$$

No allowance has been made so far for the effect that, just before the end of the water inlet pipe (i.e. the brink), the vertical velocity profile (and the water height) is non-uniform because the pressure of the water at the bottom of the inlet pipe has to decrease from $(p_a + g\rho_w h_{wi})$ to p_a, the atmospheric pressure. This is a complex problem and an approximate solution is described in Appendix 1, where it is shown that the *effective* mean inlet velocity u_i and Froude number Fr_{w_i} are enhanced by the mean hydrostatic head at the inlet pipe to give

$$u_i = k \left[\frac{M_w/2}{\rho_w h_{w_m} d} \right] \left[1 + \frac{1}{k^2 \mathrm{Fr}_{w_m}} \right]^{1/2} \quad [12a]$$

and

$$\mathrm{Fr}_{w_i} = k^3 \mathrm{Fr}_{w_m} \left[1 + \frac{1}{k^2 \mathrm{Fr}_{w_m}}\right]^{3/2} \qquad [12b]$$

where Fr_{w_m} and h_{w_m} are the Froude number $((M_w/2)/\rho_w h_{w_m} d)^2/(g h_{w_m})$ and the waterfall thickness measured just *before* the brink, k, is a constant experimentally determined later, and $\mathrm{Fr}_{w_i} = (u_i^2/g h_{w_i})$.

3.2 *The air flow*

As shown in figure 7, the air rises between the two waterfalls as if flowing in a diverging duct with flexible walls, but some will be brought to rest underneath the waterfalls. The resultant pressure difference over the water element will thus correspond to the kinetic head of the air between the waterfalls at position z. If the air flow is assumed to be one dimensional† of local velocity u_a, and if the density ρ_a of the air is assumed to be constant

$$\Delta p = \frac{1}{2} \rho_a u_a^2. \qquad [13]$$

However the air velocity u_a depends on the path followed by the air jet as it passes between the waterfalls, a complex problem in fluid mechanics.

Three possible modes of air flow between the waterfalls are illustrated in figure 8.

(i) In the first and most conservative case, illustrated in figure 8(a), it is assumed that the air follows the curvature of the waterfall, unaffected by the outlet hole of the test section, so that the air velocity at position (x, z) is given by

$$u_a = \frac{M_a}{\rho_a d(b - 2x)} \qquad [14]$$

where M_a is the mass flow rate of air, b the breadth of the test section and d the depth or gap size. Thus,

$$\Delta p = \frac{1}{2} \rho_a \left(\frac{M_a}{\rho_a d(b - 2x)}\right)^2 \qquad [15]$$

where x is measured to the centre of the water jet (jet thickness effects will be considered later).

(ii) At the opposite extreme, it is assumed that the air separates from the wall of the waterfalls, as it enters the water channel at its narrowest width $(b - 2x_b)$, at the bottom of the lower plenum, with a slow moving circulation pattern between the gas jet and the waterfall giving an approximately uniform pressure. If it is further assumed, as in figure 8(b), that the width of the air jet remains constant at the bottom value of $(b - 2x_b)$, i.e. a parallel jet, it follows that,

$$\Delta p = \frac{1}{2} \rho_a \left(\frac{M_a}{\rho_a d(b - 2x_b)}\right)^2. \qquad [16]$$

(iii) In the third case it is assumed that the air moves as a jet from the inlet of breadth $(b - 2x_b)$ to the outlet hole of effective width $\bar{d}_0$ (i.e. replacing the outlet hole with a square of

†*Note*: Three-dimensional air patterns in the tank below the test section are neglected in the analysis.

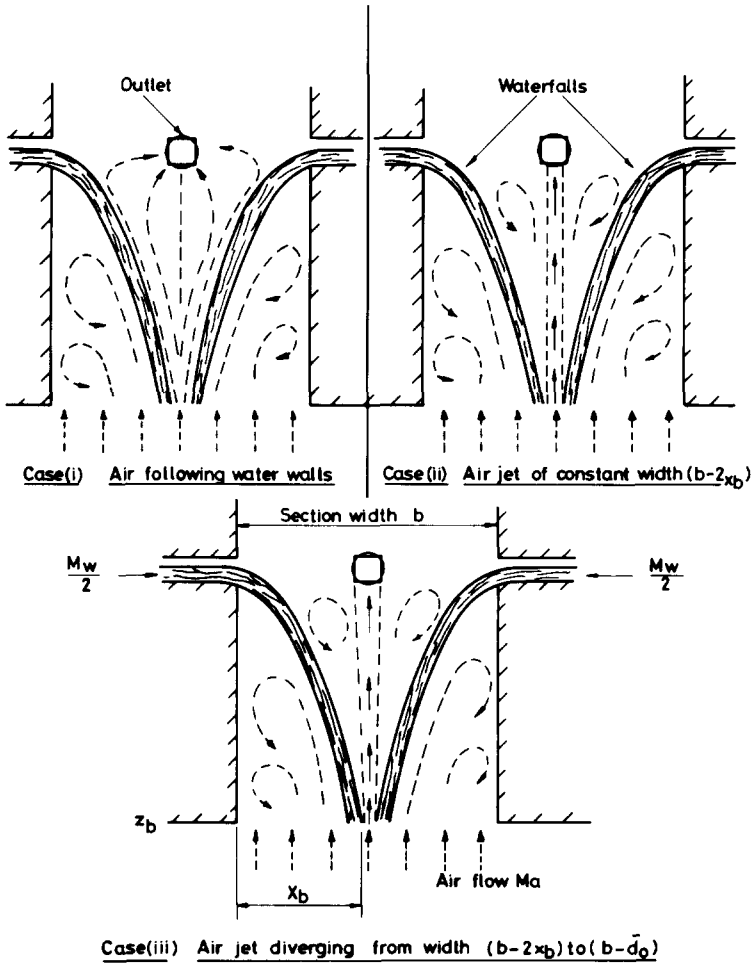

Figure 8. Possible air flow patterns.

side $\bar{d}_0$), where $\bar{d}_0 = \sqrt{(\pi/4)}\, d_0$, as shown in figure 8(c) so that

$$\Delta p = \frac{1}{2}\rho_a \left[\frac{M_a}{\rho_a d \left[\bar{d}_0 - \dfrac{\bar{d}_0 - b + 2x_b}{z_b} z \right]} \right]^2. \qquad [17]$$

In general the dimensionless pressure difference ΔP defined in [9] becomes,

$$\Delta P = \left(\frac{M_a}{M_w}\right)^2 \left(\frac{\rho_w}{\rho_a}\right) \mathrm{Fr}_{wi}^{-1} \frac{1}{(B/2 - X)^2} \qquad [18]$$

where B is the dimensionless breadth $= (2g/u_i^2)b$.

Equation [18] corresponds to [15]; if X is replaced by $X_b = (2g/u_i^2)x_b$ then the condition corresponding to [16] is obtained.

If X is replaced by $[((B/2) - (D_0/2)) + ((D_0/2 + X_b - B/2)/Z_b)Z]$, then the dimensionless form of [17] is obtained. (Here $D_0 = (2g/u_i^2)d_0$.)

3.3 *Effect of air flow on the water trajectories*

It is now possible to substitute [18] into [10] to obtain the water trajectories. For Case (i) with the air following the waterfall profile, an integral equation is obtained which can be

integrated numerically on a computer to yield dimensionless trajectories fo the form Z vs X. This has been done with the introduction of a further dimensionless parameter K where

$$K = \Delta P \left[\frac{B}{2} - X\right]^2 = \left[\frac{M_a}{M_w}\right]^2 \left[\frac{\rho_w}{\rho_a}\right] \mathrm{Fr}_{w_i}^{-1}. \qquad [19]$$

As K increases, so the ratio M_a/M_w increases thus, for the present experiments, trajectory curves for varying K values can be regarded as those relating to different upward air flow rates. A typical set of curves, for a water inlet velocity $u_i = 0.475$ m/s is shown in figure 9. As might be expected, the horizontal travel of the water increases as the air flow increases. The corresponding values of the dimensionless pressure difference ΔP at the bottom of the test section, i.e. $Z = Z_b$ are also shown in figure 9.

For Case (ii), with $\Delta P = \Delta P_b$, [10] can be integrated analytically to give,

$$X = \frac{1}{2\Delta P_b^2} \sin^{-1}[2\phi_1(R_b Z)] - \frac{1}{R_b}\phi(R_b Z) \qquad [20]$$

where the function ϕ is given by,

$$\phi(R_b Z) = (R_b Z)^{1/2}(1 - R_b Z)^{1/2} \qquad [21]$$

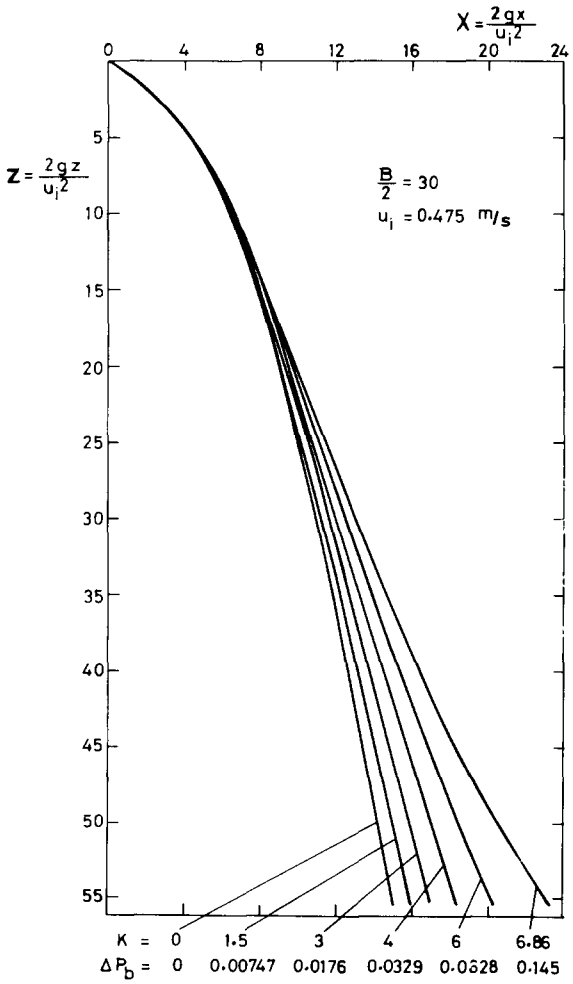

Figure 9. Dimensionless water trajectories, Case (i).

and the ratio

$$R_b = \frac{\Delta P_b^2}{1 - 2\Delta P_b}. \qquad [22]$$

It is thus possible to evaluate another family of trajectories of X vs Z, this time with a parameter ΔP_b, as shown in figure 10.

It is useful from a conceptual point of view to simplify [20] further. For the case of $\Delta P_b \ll \frac{1}{2}$ with $R_b Z \ll 1$ [20], becomes

$$X = 2Z^{1/2}(1 + \tfrac{1}{3}\Delta P_b Z) \qquad [23]$$

a perturbation of [11].

Equation [23] is also plotted in figure 10 and, again, a family of trajectories is obtained with the horizontal travel of the water increasing as the air flow (and hence ΔP_b) increases. The discrepancy between the approximation to [20] by [23] is also shown. However, if the curves shown in figure 10 are compared with those in figure 9 the horizontal travel of the water is seen to be greater in the former case, as might be expected. Perhaps what is unexpected is the magnitude of this effect; in figure 10, a $\Delta P_b \approx 0.01$ is needed for $X_b \approx 12$ compared with $\Delta P_b \approx 0.04$ in figure 9. Consequently, the two extreme assumptions embodied in the above analysis imply widely different air flow rates to give the same effect in the water trajectories.

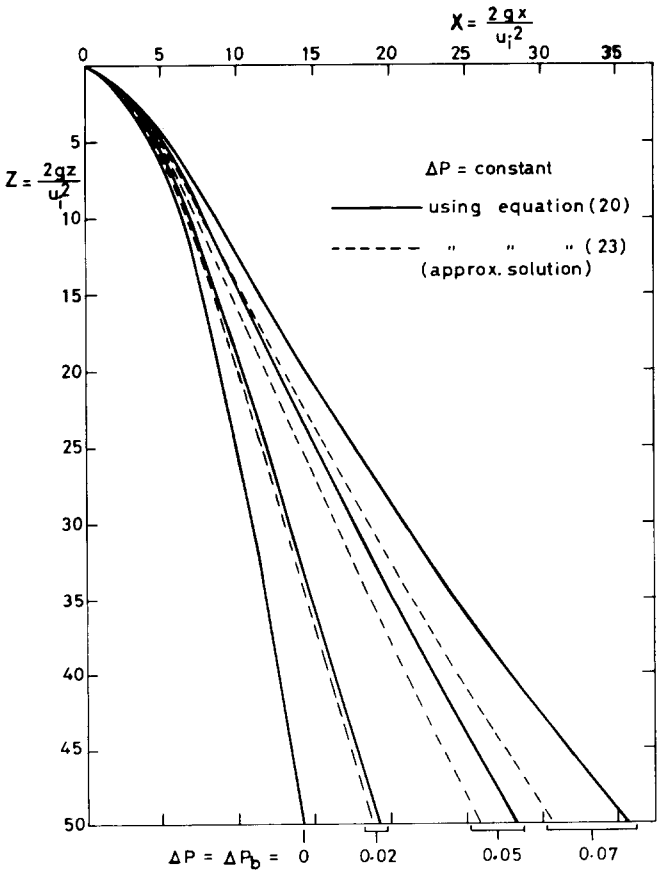

Figure 10. Dimensionless water trajectories, Case (ii).

For Case (iii) with

$$\Delta P = \frac{K}{\left[\frac{D_0}{2} - \frac{D_0/2 + X_b - B/2}{Z_b} Z\right]^2} \quad [24]$$

an integral equation is obtained of the form,

$$X = \int_0^Z \frac{dZ}{\left[\frac{1+Z}{(1+F_z)^2} - 1\right]^{1/2}} \quad [25]$$

where

$$F_z = \int_0^Z \Delta P \, dZ = \frac{KZ}{\frac{D_0}{2}\left[\frac{D_0}{2} - \frac{D_0/2 + X_b - B/2}{Z_b} Z\right]}. \quad [26]$$

This equation can be evaluated in terms of elliptic functions of the first and second kind, but it is simpler to evaluate [25] and [26] numerically on a computer.

These three numerical solutions are now exploited below.

3.4 *The condition for the collapse of the pair of waterfalls*

The condition for the collapse of the pair of waterfalls is similar for the three cases of air flow described above but can be seen most readily for the simple case of $\Delta P = \Delta P_b$ with $\Delta P_b \ll \frac{1}{2}$ corresponding to [23]. At the bottom of the test section the horizontal position of the trajectory X_b is given by [23] with $Z = Z_b$.

Choosing then a value of $Z_b = (z_b/b)B$, and remembering that for a given test section shape (b/z_b) is fixed, a curve of $X_b/(B/2)$ vs $K/(B/2)$, where K is defined by [19], can be plotted with $B/2$ as a parameter. A family of such curves is shown in figure 11(a) for values of $B/2$ between 10 and 50. Each curve can be considered to represent the theoretical predictions of the horizontal position of the water jet at the bottom of the section for a given water flow rate (M_w and u_i fixed) and a range of values of air flow rate M_a. For a given air flow rate M_a, two positions of the water jet are possible as indicated by X_b, one corresponding to a low air velocity and low value of X_b and the other corresponding to a high air velocity and a high value of X_b. Referring to figure 11(a) for any water-first type test, i.e. (fixed $B/2$), it would be expected that the water trajectory would move from position 1 towards position 2 as the air flow rate was increase, i.e. (K increased), causing the two water jets to come together. At the maximum (position 2) any further increase in air flow causes the water jets to collapse in towards one another as shown in figure 4(b). The maximum, such as that represented by position 2, corresponds to the maximum possible air flow and can be regarded as a kind of choked flow for the water jet flow pattern.

The choked flow condition can be evaluated analytically for the simple case described by [23] with $\Delta P_b = K/(B/2 - X_b)^2$. Then, since

$$\left[\frac{X_b}{B/2}\right] = 2\left[\frac{z_b}{b/2}\right]^{1/2}\left[\frac{B}{2}\right]^{-(1/2)}\left[1 + \frac{1}{3}\frac{K/\frac{B}{2}}{\left[1 - \frac{X_b}{B/2}\right]^2}\left[\frac{z_b}{b/2}\right]\right] \quad [27]$$

and if the condition $dM_a/dX_b = 0$, or $(d[(K/B/2)/d[(X_b/B/2)] = 0$, is imposed, the maximum is

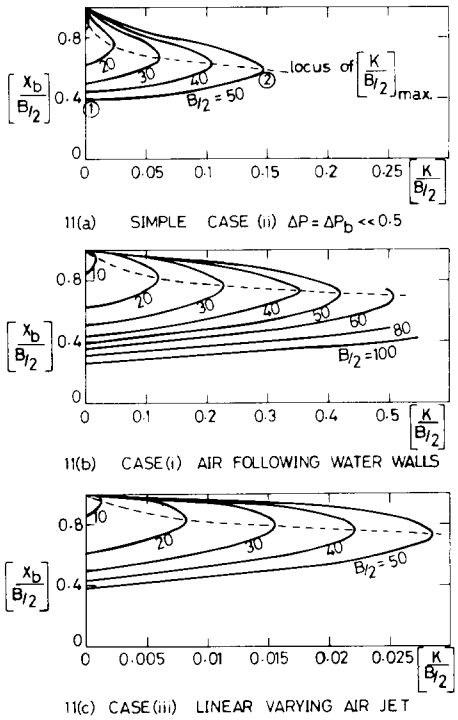

Figure 11. Position of waterfalls at bottom of test section.

found as

$$\left[\frac{X_b}{B/2}\right]_{\max} = \frac{1}{3}\left[1+4\left[\frac{z_b}{b/2}\right]^{1/2}\left[\frac{B}{2}\right]^{-(1/2)}\right] \qquad [28]$$

with

$$\left[\frac{K}{B/2}\right]_{\max} = \frac{2}{9}\left[\frac{z_b}{b/2}\right]^{-(3/2)}\left[\frac{B}{2}\right]^{1/2}\left[1-2\left(\frac{z_b}{b/2}\right)^{1/2}\left(\frac{B}{2}\right)^{-(1/2)}\right]^3. \qquad [29]$$

It is also possible to plot similar curves to those shown in figure 11(a) for the cases of the variable ΔP, using a digital computer. These are shown in figrues 11(b) and 11(c) and have the same general form.

3.5 *Choking condition*

It is worthwhile considering further the condition used above for the collapse of the pair of waterfalls, viz. $dM_a/dX_b = 0$. Consider the air flowing through cross section area A between the water jets. Then the conservation of mass gives,

$$\rho_a A u_a = M_a = \text{const.} \qquad [30]$$

and the conservation of momentum,

$$-A dp - d(\rho_a u_a^2 A) = 0 \qquad [31]$$

if frictional and gravity effects for the air are neglected. As above, the variation of ρ_a can be neglected but, in the problem considered here, A varies with the pressure p as well as position

z. Equation [31] then becomes,

$$\frac{dp}{dz} = \frac{\frac{M_a^2}{\rho_a A^3}\left[\frac{\partial A}{\partial z}\right]_p}{1 - \frac{M_a^2}{\rho_a A^3}\left[\frac{\partial A}{\partial p}\right]_z} \quad [32]$$

where the denominator term

$$\frac{M_a^2}{\rho_a A^3}\left[\frac{\partial A}{\partial p}\right]_z = (\text{Mach number})^2.$$

Choking occurs when $(dp/dz) \to \infty$, implying,

$$\left[\frac{M_a}{\rho_a A}\right]^2 = \frac{A}{\left(\frac{\partial A}{\partial p}\right)_z} = C_a^2 = (\text{sonic velocity})^2. \quad [33]$$

In this equation it is assumed that the effect of pressure on the density of the air is small compared with its effect on the area between the waterfalls. In [32] and [33] the Mach number and sonic velocity terms are equivalent to those used in gas dynamics but with the gas compressibility effects small compared with area change effects.

Since $\Delta p = p_a - p = \frac{1}{2}\rho_a C_a^2$, [33] can be rewritten as

$$\Delta p = -\tfrac{1}{2}\frac{A}{\left[\frac{\partial A}{\partial p}\right]_z} \quad [34]$$

or

$$\frac{\partial(\Delta p^{1/2} A)}{\partial A} = 0. \quad [35]$$

Now $\Delta p^{1/2} A \propto K^{1/2}$ and $dA \propto -dX_b$. Thus [35] becomes $(dK^{1/2}/dX_b) = 0$ or $(dM_a/dX_b) = 0$. Thus the criterion used to give the collapsing of the pair of waterfalls is equivalent to that for choked flow in [33]. It can be shown (Appendix 2) that the corresponding "sonic" velocity given by [33] is about 3 m/s, very much less than the velocity of sound in still air at the same temperature and pressure. This is probably due to the flexibility of the restraining water jets causing an area change and hence changing the $\partial A/\partial p$ term.

3.6 *The collapse condition in terms of j_s^* and j_w^**

Equations [19] and [29] can be written in a form suitable for making comparison with the experimental data by noting that

$$Z_b = 2^{5/3} \mathrm{Fr}_{w_i}^{-(2/3)} \mathrm{Fr}_{wb}^{-(1/3)} \left(\frac{z_b}{b}\right); \quad B = 2^{5/3} \mathrm{Fr}_{wi}^{-(2/3)} \mathrm{Fr}_{w_b}^{-(1/3)} \quad [36]$$

where

$$\mathrm{Fr}_{w_b} = \left[\frac{M_w\, db}{\rho_w}\right]^2 \Big/ gb. \quad [37]$$

Thus

$$\left[\frac{M_a}{M_w}\right]^2 = \frac{\sqrt{2}}{9}\left[\frac{\rho_a}{\rho_w}\right]\left[(\mathrm{Fr}_{w_b})^{-(1/6)}\left(\frac{b}{z_b}\right)^{1/2} - 2^{7/6}(\mathrm{Fr}_{wi})^{1/3}\right]^3. \quad [38]$$

Alternatively this can be written in terms of j_a^* and j_w^* where

$$j_a^* = \frac{M_a}{\rho_a bd} \cdot \frac{\rho_a^{1/2}}{[gb(\rho_w - \rho_a)]^{1/2}} \approx (\mathrm{Fr}_{ab})^{1/2}\left(\frac{\rho_a}{\rho_w}\right)^{1/2} \quad [39]$$

$$\mathrm{Fr}_{ab} = \left[\frac{M_a\, db}{\rho_a}\right]^2 \Big/ gb,$$

and

$$j_w^* = \frac{M_w}{\rho_w bd} \cdot \frac{\rho_w^{1/2}}{[gb(\rho_w - \rho_a)]^{1/2}} \approx \mathrm{Fr}_{wb}^{1/2} \quad [40]$$

to give

$$[j_a^* \mathrm{Fr}_{wi}^{1/2}]^2 = \frac{\sqrt{2}}{9}(j_w^* \mathrm{Fr}_{wi})\left[\left(\frac{b}{z_b}\right)^{1/2} - 2^{7/6}(\mathrm{Fr}_{wi} j_w^*)^{1/3}\right]^3. \quad [41]$$

A plot of $(j_a^* \mathrm{Fr}_{wi}^{1/2})$ vs $(j_w^* \mathrm{Fr}_{wi})$ for the test section geometry is shown in figure 12. It is, of course, possible to transform the curves in figure 11(a) directly.

In a similar manner, it is possible to transform the collapse condition shown in figures 11(b) and 11(c) using [36]–[40] to give curves of $j_a^* \mathrm{Fr}_{wi}^{1/2}$ vs $j_w^* \mathrm{Fr}_{wi}$. These curves are also plotted in figure 12. For Case (iii), a further refinement used was to take the two dimensional equivalent of the outlet hole to be given by

$$\bar{d}_0 = \sqrt{\left(\frac{\pi}{4}\right)} \cdot d_0, \quad \text{i.e. area} = \bar{d}_0^2 = \frac{\pi}{4} d_0^2.$$

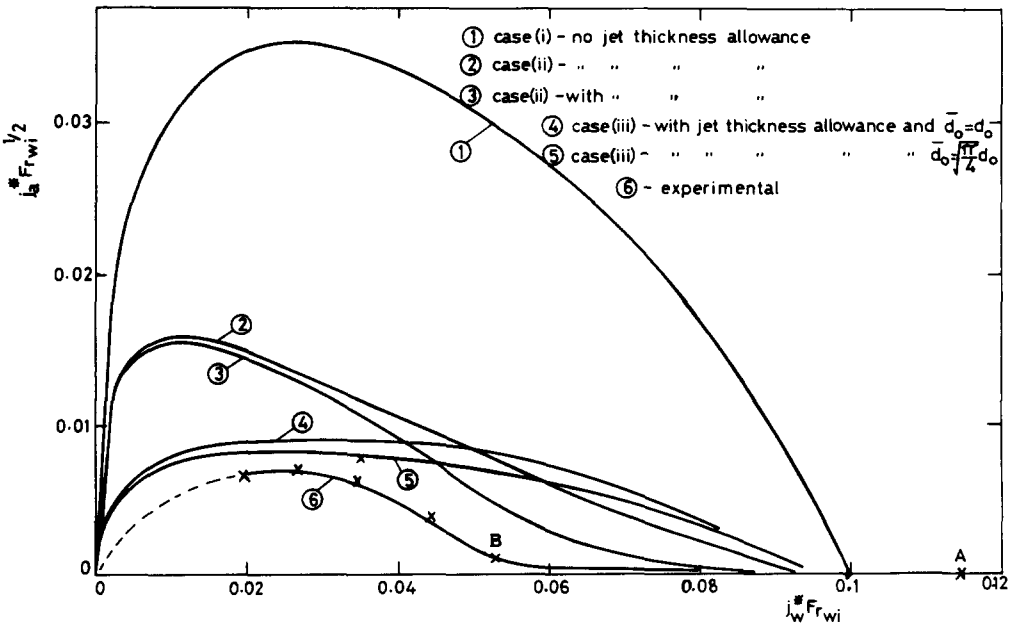

Figure 12. Comparison between theory and experiment—collapse condition for waterfall pair.

3.7 *Allowance for the thickness of the waterfalls*

In the previous analysis, the effect of the thickness of the waterfall on the area available for the passage of air has been neglected. This is a good assumption near the top of the test section, but near the bottom, particularly when $(X_b/B/2) > 0.9$, a correction may be made. Details of this correction are shown in Appendix 3. The calculations described previously was carried out with this correction factor and the results also plotted in figure 12.

4. COMPARISON BETWEEN THEORY AND EXPERIMENT

4.1 *Water trajectories with zero air flow*

Measurements were taken of the centre position of the water jet trajectories for zero air flow and various water flows and curves are shown in figure 5, as was mentioned earlier. The three typical curves shown relate to water inlet conditions such that the Froude number Fr_{w_m}, measured just before the brink, were 1.49, 1.41, 1.375 and 1.118 and the flowrate per side (i.e. $M_w/2$) were 0.275, 0.395, 0.613 and 1.12 kg/s, respectively.

According to the above theory, the trajectory is given by [11] which can be rewritten as

$$x = \left(\frac{2}{g}\right)^{1/2} u_i z^{1/2} \qquad [42]$$

or using [12a], and eliminating h_{wm},

$$x = \sqrt{\left(\frac{2}{g}\right)} k \left[\frac{gM_w \mathrm{Fr}_{w_m}}{2d\rho_w}\right]^{1/3} \left[1 + \frac{1}{k^2 \mathrm{Fr}_{w_m}}\right]^{1/2} z^{1/2}. \qquad [43]$$

A value of $k = 0.819$ was found to fit the experimental data for all the trajectories, giving $x = 11.6z^{1/2}$, $10.05z^{1/2}$ and $8.95z^{1/2}$ with x and z in mm. The agreement between theory and experiment is very good bearing in mind that only one adjustable parameter k was used, the complexity of the brink flow, and the fact that no allowance was made for drag on the walls of the test section.

4.2 *Condition for the collapse of the pair of waterfalls*

The experimental values of the air flow rate M_a at which the two water jets collapse towards one another for a given water flow are plotted on figure 6 with the corresponding values of j_a^*, j_w^* and Fr_{w_m} listed in table 1. The corresponding values of Fr_{w_i} according to [12b] are also shown in table 1, along with the parameters $\mathrm{Fr}_{w_i}^{1/2} j_a^*$ and $\mathrm{Fr}_{w_i} j_w^*$. These last two parameters are compared with the theoretical curves in figure 12.

The first point to note from figure 12 is that the theoretical curves and a line through the experimental points are qualitatively of the same shape but that all the theories predict a higher value of air flow required for waterfall collapse. The theory predicts $j_a^* \mathrm{Fr}_{w_i}^{1/2} = 0$ for $j_w^* \mathrm{Fr}_{w_i} = 0$ and $j_w^* \mathrm{Fr}_{w_i} \approx 0.1$; the former corresponds to the case of the waterfall thickness being infinitesimally thin for finite Fr_{w_i} and the latter to the two waterfalls meeting in the centre of the test section without any assistance from the air. Unfortunately, experimental values below $j_w^* \mathrm{Fr}_{w_i} = 0.015$ could not be obtained since, at these low values, the flow of air caused the sluggish waterfalls to part, giving a film flow as shown in figure 4(c).

The second point to note is how small a value of $j_a^* \mathrm{Fr}_{w_i}^{1/2}$ is required (even at the maximum) for the waterfall collapse. The experimental data give a maximum value of $j_a^* \mathrm{Fr}_{w_i}^{1/2} \approx 0.007$ compared with the theoretical values of (i) 0.035 for the case of the air jet following the contours of the waterfall, (ii) 0.016 for the case of $\Delta P = \Delta P_b$, a constant, and (iii) 0.008 for the case of the linear air jet with due allowance made for waterfall thickness. Clearly, the linear air jet theory gives best agreement with experiment, at least when $j_w^* \mathrm{Fr}_{w_i} < 0.047$, i.e. where the outlet hole size $\bar{d}_0$ equals the waterfall gap $(b - 2x_b)$ at the bottom. For values of $j_w^* \mathrm{Fr}_{w_i} > 0.047$,

Table 1. Experimental values relating to the collapse condition of the pair of waterfalls water first tests

M_w kg/s	M_a kg/s	j_w^*	j_a^*	Fr_{w_m}	Fr_{w_i}	$Fr_{w_i}^{\frac{1}{2}} j_a^*$	$Fr_{w_i} j_w^*$
0.536	0.00756	0.0118	0.0047	1.32	2.26	0.0071	0.0267
0.712	0.000658	0.0156	0.0042	1.28	2.24	0.0063	0.0349
0.884	0.00409	0.0194	0.0026	1.41	2.29	0.0039	0.0444
1.057	0.0013	0.0232	0.0008	1.35	2.27	0.0012	0.0527
0.40	0.0073	0.0088	0.0045	1.35	2.27	0.0068	0.02
0.702	0.0083	0.0154	0.0052	1.35	2.27	0.0078	0.035
1.056	0.0013	0.0232	0.0008	1.35	2.27	0.0012	0.0527
2.23	0	0.0489	0	1.118	2.19	0	0.1071

$$Fr_{w_i} = 0.55\, Fr_{w_m}\left[1 + \frac{1}{0.67\, Fr_{w_m}}\right]^{3/2}$$

i.e. high water flow rates, the theory with $\Delta P = \Delta P_b$ is closest to the experimental data, a not too surprising effect since the air jet will certainly separate from the waterfall and not follow the linear divergence to the outlet hole. The importance of the waterfall thickness is also evident in figure 12 when $j_w^* Fr_{w_i} > 0.047$.

The air flows at these higher values of waterflow are very small, so much so that the mere shutting of the drain valve from the bottom tank, resulting in a small flow of displaced air, was enough to move point A to point B, in figure 12. The theory predicts this sensitivity in a satisfactory way.

Thus it is concluded that the linear air jet theory explains the theoretical data up to the waterflow rates at which $\bar{d}_0 = (b - 2x_b)$ whilst beyond that the $\Delta P = \Delta P_b$ theory gives the best fit. At the maximum, the theory exceeds the experiment by about 15 per cent, reasonable agreement when the complexity of the flow and the simplifications of the theory are considered. It seems likely that, in water first tests (fixed $B/2$) as the air flow is increased (K increased), i.e. along the lower position of one of the curves in figure 11, the possibility of jumping to the upper portion of the curve will increase as the maximum K value is reached. It is thus likely that the experimental values shown on figure 12 were not true collapse points but somewhat less than the maximum value. Indeed, on occasions, a fluttering of the waterfall position was noted as the air passed between them.

Finally, it must be emphasized again, that the collapse condition analysed above occurs at air flow rates far below the bypass condition of interest in the PWR refill problem. For example, the maximum value of $j_a^* Fr_{w_i}^{1/2} = 0.007$ in figure 12, is very much less than the corresponding value of $j_a^* Fr_{w_i}^{1/2} \approx 0.13$ at $j_w^* Fr_{w_i} = 0.03$ found for the start of bypass and 0.3 for complete bypass (Simpson & Rooney 1980).

5. CONCLUSIONS

The theory outlined above gives a satisfactory explanation of the collapse of the pair of waterfalls when air flows upwards between them, bearing in mind the complexity of the flow of the air stream and the proximity of the walls of the test section.

Acknowledgement—The authors gratefully acknowledge the financial and other assistance received from the U.K. Nuclear Installations Inspectorate.

REFERENCES

MARKLAND, E. 1965 Calculation of flow at a free overfall by relaxation method. *Proc. Inst. Civil Engrs* **31**, 71–78.

ROONEY, D. H., SIMPSON, H. C. & CAMPBELL, T. 1977 PWR refill studies. *Instit. Mech. Engrs Conf. Heat and Fluid Flow in Water Reactor Safety*, Manchester, England, pp. 167–173.

SIMPSON, H. C. & ROONEY, D. H. 1980 An investigation of flooding phenomena in an experiment related to the PWR problem. *Nuclear Reactor Thermal-Hydraulics Topical Meeting*, ANS/ASME, Saratoga.

APPENDIX 1

Flow over the brink into the test section

As the water in the inlet pipe approaches the entrance to the test section, the hydrostatic head has to adjust such that, after the water flows over the brink, the pressure on the underside of the jet becomes uniform and atmospheric. This is a complex problem which has been studied extensively by Civil Engineers and normally requires numerical integration of the fluid flow equations for the water jet. This integration has been done by Markland (1965) who studied the ideal problem of flow of a stream initially with uniform velocity u, over a brink. The velocity, pressure and energy profiles at three stations (upstream, brink and downstream) are indicated in figure A1. It can be seen that as the water at section 1 approaches the brink at section 2, it accelerates and thus, by continuity, the surface height decreases. At section 1, the velocity profile is flat and the pressure and surface increase linearly from top to bottom of the water jet. At section 2 the pressure at the bottom of the channel has dropped to atmospheric, leaving a pressure maximum inside the water jet, and the velocity distribution increases in a non-linear manner from the top to bottom although the energy distribution is still linear. At section 3, the velocity distribution is again flat and the pressure uniformly atmospheric.

The effect of the hydrostatic head at section 1 therefore is to accelerate the fluid at section 2. There is however a residual pressure potential which can accelerate the water further.

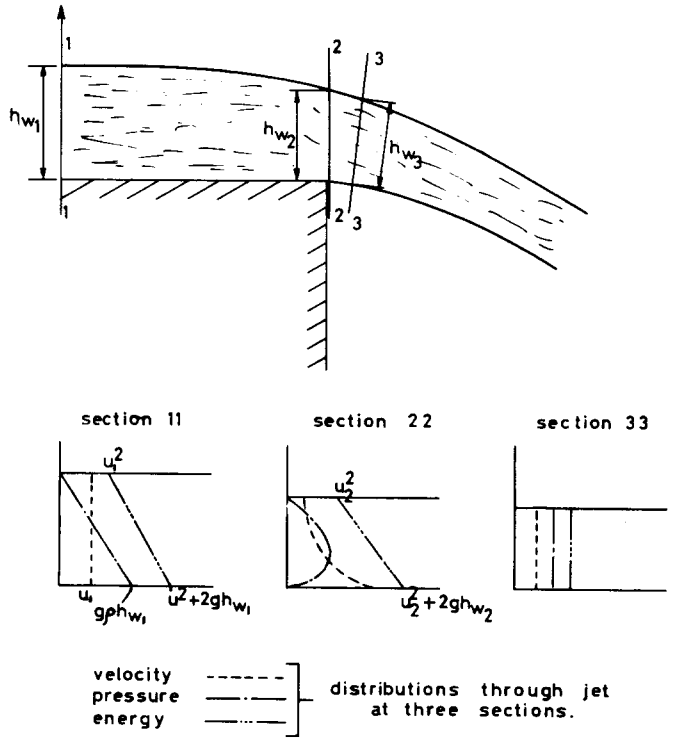

Figure A1. Representation of idealised flow over a brink.

In the actual experiments the flow patterns were more complex. The water was fed to the side arms down a vertical pipe resulting in an undulating surface initially as shown in figure A2. However, the decrease in water depth (and hence the increase in Froude number) is apparent as the brink is approached. Because of the complexity of the real flow and the non-linear aspects of the above theory, a simplified analysis was made to estimate the effective water jet velocity just after the brink, based on the measured total mass flow M_w of the inlet water and the measured water depth h_{w_2} at section 2.

At section 2, the energy varies linearly from u_2^2 to $(u_2^2 + 2gh_{w_2})$ and the square of the velocity varies in a non-linear manner between these two limits. Thus the mean energy at section 2, $\bar{E}_2$, is given by,

$$\bar{E}_2 = u_2^2 + gh_{w_2}.$$

The term u_2^2 will be somewhat less than the corresponding mean velocity term $\bar{u}_2^2$, but this will be taken care of in a correction factor k^2. Thus, writing an energy balance on the fluid between section 2 and 3 (section 3 close to 2), where the velocity u_3 is assumed uniform at constant atmospheric pressure and channel height h_{w_3}, gives

$$\bar{u}_2 h_{w_2}[k^2\bar{u}_2^2 + gh_{w_2}] = \bar{u}_3 h_{w_3}\bar{u}_3^2. \qquad \text{[A1-1]}$$

By continuity

$$\bar{u}_2 h_{w_2} = \bar{u}_3 h_{w_3}. \qquad \text{[A1-2]}$$

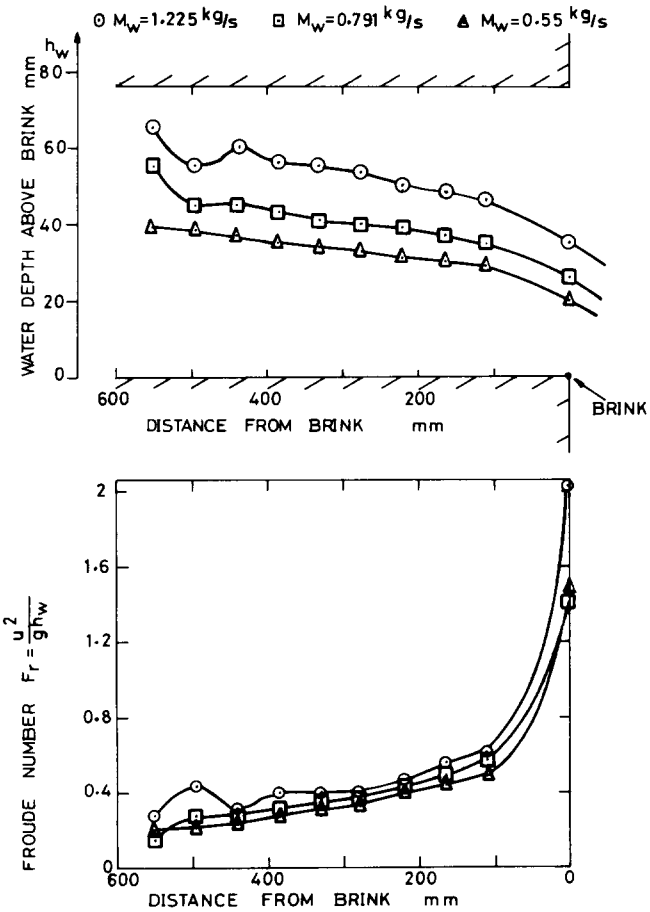

Figure A2. Experimental values of water depth and Froude number approaching brink of test section.

Thus,

$$\bar{u}_3^2 = k^2\bar{u}_2^2 + gh_{w_2} \qquad [A1\text{-}3]$$

giving

$$\bar{u}_3^2 = k^2\bar{u}_2^2\left[1+\frac{1}{k^2\mathrm{Fr}_{w_2}}\right] \qquad [A1\text{-}4]$$

where

$$\mathrm{Fr}_{w_2} = \frac{\bar{u}_2^2}{gh_w^2} \quad \text{and} \quad k^2 = \frac{u_2^2}{\bar{u}_2^2}. \qquad [A1\text{-}5]$$

It is also possible to estimate the channel height h_{w_3} as,

$$h_{w_3} = \frac{\bar{u}_2 h_{w_2}}{\bar{u}_3} = \frac{\bar{u}_2 h_{w_2}}{k\bar{u}_2\left[1+\frac{1}{k^2\mathrm{Fr}_{w_2}}\right]^{1/2}} = \frac{h_{w_2}}{k\left[1+\frac{1}{k^2\mathrm{Fr}_{w_2}}\right]^{1/2}}. \qquad [A1\text{-}6]$$

Thus,

$$\mathrm{Fr}_{w_3} = \frac{\bar{u}_3^2}{gh_{w_3}} = k^3\mathrm{Fr}_{w_2}\left[1+\frac{1}{k^2\mathrm{Fr}_{w_2}}\right]^{3/2} \qquad [A1\text{-}7]$$

Using the nomenclature of the main part of the paper, the effective u_i and Fr_{w_i} just after the brink is given by,

$$u_i = k\left[\frac{M_w/2}{\rho_w d h_{wm}}\right]\left[1+\frac{1}{k^2\mathrm{Fr}_{w_m}}\right]^{1/2} \qquad [A1\text{-}8]$$

and

$$\mathrm{Fr}_{w_i} = k^3\mathrm{Fr}_{w_m}\left[1+\frac{1}{k^2\mathrm{Fr}_{w_m}}\right]^{3/2}. \qquad [A1\text{-}9]$$

From the experimental data, k was found subsequently to be 0.819.

APPENDIX 2

Evaluation of air velocity at choking condition

At choking

$$u_a = \frac{M_a}{\rho_a d(b-2x)} = \frac{M_a}{\rho_a d}\cdot\frac{2g}{u_i^2}\cdot\frac{1}{\mathrm{B}(1-\eta_b)} \qquad [A2\text{-}1]$$

where

$$\eta_b = \frac{2X_b}{B}.$$

Now

$$K = \left[\frac{M_a}{M_w}\right]^2 \left[\frac{\rho_w}{\rho_a}\right] \mathrm{Fr}_{w_i}^{-1} \quad \text{from [19]}$$

with

$$u_i^2 = g h_{w_i} \mathrm{Fr}_{w_i} = g \mathrm{Fr}_{w_i} \left[\frac{M_w}{2 d \rho_w u_i}\right] = g \mathrm{Fr}_{w_i}^{2/3} \left[\left\{\frac{M_w}{2\rho_w d}\right\}^2 \cdot \frac{1}{g}\right]^{1/3} \qquad \text{[A2-2]}$$

hence from [A2-1]

$$u_a = \frac{M_w K^{1/2} \left[\frac{\rho_a}{\rho_w}\right]^{1/2} \mathrm{Fr}_{w_i}^{1/2}}{\rho_a d} \cdot \frac{2g}{g \mathrm{Fr}_{w_i}^{2/3} \left[\left\{\frac{M_w}{2\rho_w d}\right\}^2 \frac{1}{g}\right]^{1/3}} \cdot \frac{1}{B(1-\eta_b)}. \qquad \text{[A2-3]}$$

Now

$$\mathrm{Fr}_{w_b} = \left[\frac{M_w}{\rho_w b d}\right]^2 \cdot \frac{1}{gb}$$

giving

$$\left[\frac{M_w}{2\rho_w d}\right]^2 = \frac{\mathrm{b}^3 \mathrm{Fr}_{w_b}}{4} \qquad \text{[A2-4]}$$

and from [36]

$$\mathrm{Fr}_{w_b}^{1/3} = \frac{2^{5/3}}{B \mathrm{Fr}_{w_i}^{2/3}} \qquad \text{[A2-5]}$$

hence from [A2-3]

$$u_a = 2\left[\frac{K}{B/2}\right]^{1/2} \left[\frac{1}{1-\eta_b}\right] \left[\frac{\rho_w}{\rho_a}\right]^{1/2} \left[\frac{gb}{\mathrm{Fr}_{w_i}}\right]^{1/2} \left[\frac{1}{B/2}\right]. \qquad \text{[A2-6]}$$

For this work

$$\sqrt{(gb)} = \sqrt{(9.81 \times 0.69)} = 2.602 \text{ m/s}, \quad \rho_w = 1000 \text{ kg/m}^3, \quad \rho_a \approx 1.308 \text{ kg/m}^3 \quad \mathrm{Fr}_{w_i} \approx 2.2$$

hence

$$u_a \approx 97 \left[\frac{K}{B/2}\right]^{1/2} \left[\frac{1}{1-\eta_b}\right] \left[\frac{1}{B/2}\right] \quad \text{where} \quad \eta_b = \frac{X_b}{B/2}.$$

A typical value of $B/2$ during the tests was 20 and, from figure 11(c), this gives corresponding values of $[K/(B/2)] \approx 0.0085$ and $(X_b/(B/2)) \approx 0.84$ hence $u_a = 97 \times 0.00085 \times (1/(0.16 \times 20)) \approx 2.8$ m/s.

APPENDIX 3

Allowance for the thickness of the waterfalls

The waterfall thickness has two effects, (*a*) it increases Z_b by $h_{wi}/2$, (b) it decreases the air passage width by $h'_w = (h_w/\cos\theta)$ or, in dimensionless form, by $H'_w = [2_g h_w/u_i^2](1/\cos\theta)$.

From [3] and [6]

$$H'_w = \left[\frac{2g}{u_i^2}\right]\frac{h_{w_i}u_i}{\bar{v}} \cdot \frac{\bar{v}}{u_i\left[\left(1+\frac{2gz}{u_i^2}\right)-\left(1+\frac{1}{\rho_w h_{w_i} u_i^2}\int_0^z \Delta p\, dz\right)^2\right]^{1/2}}.$$

Now consider the value of $H_w = H_{wb}$ where $z = z_b$ (where the correction is important) and for simplicity assume there that $\cos\theta \approx 1$

$$H_{wb} = \frac{2g}{u_i^2} \cdot \frac{h_{w_i}u_i}{[2_g z_b + u_i^2]^{1/2}} = \frac{2}{\mathrm{Fr}_{w_i}} \cdot \frac{1}{(1+Z_b)^{1/2}}. \qquad \text{[A3-1]}$$

This correction was applied to the whole of the waterfall.

Thus in the previous calculations Z_b was replaced by Z'_b and $B/2$ by $B'/2$ where

$$Z'_b = Z_b + \frac{2g}{u_i^2} h_{w_i} = Z_b + \frac{2}{\mathrm{Fr}_{w_i}} \qquad \text{[A3-2]}$$

and

$$\frac{B'}{2} = \frac{B}{2} - \frac{1}{\mathrm{Fr}_{w_i}(1+Z_b)^{1/2}}. \qquad \text{[A3-3]}$$